AIAA 79-1620R

Singular Perturbation Techniques for On-Line Optimal Flight-Path Control

Anthony J. Calise*
Drexel University, Philadelphia, Pa.

This paper presents a partial evaluation on the use of singular perturbation methods for developing computer algorithms for on-line optimal control of aircraft. The evaluation is based on a study of the minimum time intercept problem using F-4 aerodynamic and propulsion data as a base line. The extensions over previous work on this subject are that aircraft turning dynamics (in addition to position and energy dynamics) are included in the analysis, the algorithm is developed for a moving end point and is adaptive to unpredictable target maneuvers, and short-range maneuvers that do not have a cruise leg are included. Particular attention is given to identifying those quantities that can be precomputed and stored (as a function of aircraft total energy), thus greatly reducing the on-board computational load. Numerical results are given that illustrate the nature of the optimal intercept flight paths, and an estimate is given for the execution time and storage requirements of the control algorithm.

Nomenclature

C_D = drag coefficient
C_{D0} = drag coefficient for $\alpha = 0$
C_L = lift coefficient
C_{L_α} = slope of lift coefficient curve, 1/rad
D = drag, lb
D_0 = drag for $L = W$, lb
E = total energy per unit weight, ft
E_0 = long-range cruise energy level, ft
E_0^* = pseudo-cruise energy level, ft
G = load factor
g = gravitational constant, ft/s^2
H = Hamiltonian
h = altitude, ft
K = induced drag parameter
K_1, K_2, K_3 = gains, 1/s
L = lift, lb
L_n = horizontal lift component, lb
L_σ = vertical lift component, lb
M = Mach number
m = mass, slug
P_E = energy state and co-state eigenvalues, 1/s
P_β = heading state and co-state eigenvalues, 1/s
q = dynamic pressure, lb/ft^2
R = range, ft
s = reference area, ft^2
T = thrust, lb
t = time
t_{go} = time-to-go, s
V = velocity, ft/s
W = weight, lb
x, y = target-centered horizontal axes, ft
α = angle of attack, rad
β = heading, rad
γ = flight-path angle, rad
$\delta(-)$ = perturbation associated with a particular variable
ϵ = perturbation parameter
η = induced drag parameter
γ_d = desired flight-path angle, rad
λ = line-of-sight angle, rad
λ_E = energy co-state, s/ft
λ_x, λ_y = position co-states, s/ft
λ_β = heading co-state, s/rad
μ = bank angle, rad
ρ = air density, slug/ft^3
τ = stretched time scale, s

Subscripts

C = climb
D = descent
f = final
max = maximum
min = minimum
T = target
0 = outer solution variable or solution
$1,2$ = boundary-layer variables or solution

Superscripts

c = climb
d = descent
$\bar{(\ )}$ = nominal value

Introduction

In general, problems in aircraft optimal flight-path control require the solution of nonlinear two-point boundary-value problems. Many authors have used reduced-order modeling techniques such as energy state approximations to circumvent this difficulty.[1-4] However, these solutions are restrictive in that either turning or position dynamics are ignored,[2,4] or assumptions are made concerning the existence of a cruise point as part of the optimal trajectory.[1,3] Under varying sets of assumptions, algorithms are developed that can be used for on-line control.

It has been shown that singular perturbation methods are useful for extending energy state modeling approaches to more general problem formulations.[5] These methods constitute a reduced-order analysis approach where the system dynamics are separated into slow and fast modes. This permits the solution of high-order problems to be approximated by the solution of a series of lower-order problems. This procedure has been applied to several problems in flight mechanics[6-8] and has resulted in algorithms that have a nonlinear feedback form. Assuming appropriate measurements are available, these algorithms are useful for on-board vehicle control.

Presented as Paper 79-1620 at the AIAA Atmospheric Flight Mechanics Conference, Boulder, Colo., Aug. 6-8, 1979; submitted Nov. 16, 1979; revision received Dec. 17, 1980.

*Associate Professor, Mechanical Engineering and Mechanics. Member AIAA.

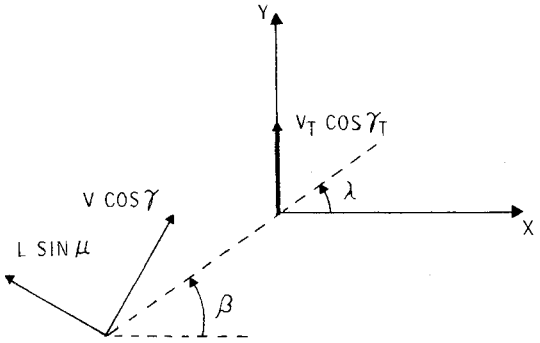

Fig. 1 Horizontal projection of the intercept geometry.

This paper investigates the use of singular perturbation methods to develop a real-time algorithm for minimum-time intercept. Emphasis is placed on deriving a solution in a form that minimizes on-board computational requirements.

Problem Formulation

The equations of motion are written in a horizontal, target-centered coordinate frame:

$$\dot{x} = V\cos\gamma\cos\beta \qquad \dot{y} = V\cos\gamma\sin\beta - V_T\cos\gamma_T \tag{1}$$

$$\dot{E} = (T-D)V/W \qquad \dot{\beta} = L\sin\mu/mV\cos\gamma \tag{2}$$

$$\dot{h} = V\sin\gamma \qquad \dot{\gamma} = (L\cos\mu - W\cos\gamma)/mV \tag{3}$$

The variables in Eqs. (1-3) are defined with the aid of Fig. 1, where the subscript "T" is used to designate the target. These equations are valid for a flat Earth, with thrust directed along the flight-path and weight constant. Drag is assumed to have a conventional parabolic form

$$D = qsC_D = qs(C_{D_0} + \eta C_{L_\alpha}\alpha^2) \tag{4}$$

which can also be written as

$$D = qsC_D + KL^2/qs \qquad q = \tfrac{1}{2}\rho V^2 \tag{5}$$

where

$$K = \eta/C_{L_\alpha} \qquad L = qsC_L = qs(C_{L_\alpha}\alpha) \tag{6}$$

The variable E is the total aircraft energy (kinetic and potential) per unit weight

$$E = h + V^2/2g \tag{7}$$

The control variables are aircraft lift, bank angle, and thrust. The objective is to find the controls L, μ, and T that minimize

$$J = \int_0^{t_f} dt \tag{8}$$

subject to the following state and control variable constraints:

$$L \le WG_{\max} \qquad L \le qsC_{L_\alpha}\alpha_{\max} \tag{9}$$

$$T_{\min}(h,M) \le T \le T_{\max}(h,M) \tag{10}$$

$$q \le q_{\max} \qquad M \le M_{\max}(h) \tag{11}$$

where $T_{\min}$ and $T_{\max}$ are functions of aircraft altitude and Mach. The boundary conditions are such that the initial aircraft state is fully specified and we require

$$x(t_f) = y(t_f) = 0 \qquad h(t_f) = h_T(t_f) \tag{12}$$

for intercept, where $h_T(t_f)$ is taken as a projected target motion in altitude

$$h_T(t_f) = h_T(0) + (V_T\sin\gamma_T)t_f \tag{13}$$

Singular Perturbation Analysis

In the analysis that follows, it is assumed that γ and $\dot{\gamma}$ are small. Hence, we set

$$\gamma = 0 \qquad L\cos\mu = W \tag{14}$$

and adopt h as an additional control variable. The objective here is to use singular perturbation methods to approximate the open-loop optimal control solution with a near-optimal, nonlinear control solution in feedback form. Toward this end, the equations of motion in Eqs. (1) and (2) are scaled by powers of ϵ:

$$\dot{x} = V\cos\beta \qquad \dot{y} = V\sin\beta - V_T\cos\gamma_T \tag{15}$$

$$\epsilon\dot{E} = (T-D)V/W \qquad \epsilon^2\dot{\beta} = L_n/mV \tag{16}$$

where $L_n \equiv L\sin\mu$. Here we seek to approximate the solution for $\epsilon = 1.0$ by an expansion about $\epsilon = 0$, with the hope that only zero-order terms are required. This ordering implies that energy state dynamics are faster than position dynamics but slower than heading dynamics. It is possible to relate the parameter ϵ to physical parameters by appropriately normalizing the equations of motion, and it can be shown that this scaling is appropriate for sufficiently long-range trajectories and for aircraft with moderate energy rate dynamics. Physically, long-range trajectories imply the existence of a near-constant altitude-constant velocity cruise arc. Climbs and descents are viewed as boundary layer transitions in energy that take place over narrow portions of the trajectory close to the initial and final times. For moderate energy rates, turning takes place at near-constant energy. The Appendix further justifies this ordering.

Necessary Conditions

In addition to Eqs. (15), (16) and the constraints in Eqs. (9-14), we have the following necessary conditions for optimality:

$$\dot{\lambda}_x = -\partial H/\partial x = 0 \qquad \dot{\lambda}_y = -\partial H/\partial y = 0 \tag{17}$$

$$\epsilon\dot{\lambda}_E = -\partial H/\partial E \qquad \epsilon^2\dot{\lambda}_\beta = -\partial H/\partial\beta \tag{18}$$

$$L,T,h = \arg\{\min_{L,T,h} H(\boldsymbol{x},\boldsymbol{\lambda},\boldsymbol{\mu})\} \tag{19}$$

where the minimization in Eq. (19) is subject to the constants in Eqs. (9-11) and (14), $\boldsymbol{x}$ is the state vector, $\boldsymbol{\lambda}$ the adjoint vector, $\boldsymbol{\mu}$ the control vector, and

$$H = \boldsymbol{\lambda}^T\dot{\boldsymbol{x}} + 1 + \text{constraints} = 0 \tag{20}$$

The vector $\dot{\boldsymbol{x}}$ represents the right-hand sides of Eqs. (15) and (16).

Outer Solution

Taking the limit $\epsilon \to 0$ in Eqs. (16) and (18) we have the following zero-order necessary conditions for the outer solution:

$$T_0 = D_0 \qquad L_{n_0} = 0 \tag{21}$$

$$\partial H_0/\partial E = \partial H_0/\partial h = \partial H_0/\partial\beta = 0 \tag{22}$$

$$H_0 = \lambda_x V\cos\beta + \lambda_y[V\sin\beta - V_T\cos\gamma_T] + 1 + \text{constraints} = 0 \tag{23}$$

We note from Eqs. (22) and (23) that the original control variables L and μ have been replaced by the fast variables E and β. From Eq. (22) we have

$$\partial H_0/\partial\beta = -\lambda_x V\sin\beta + \lambda_y V\cos\beta = 0 \tag{24}$$

or that

$$\tan\beta = \lambda_y/\lambda_x \tag{25}$$

Hence, the optimal intercept heading is constant, since from Eq. (17) λ_x and λ_y are constant. In order to satisfy the intercept requirement, β must satisfy (see Fig. 1)

$$V\sin(\beta-\lambda) = V_T\cos\gamma_T\cos\lambda \tag{26}$$

where λ is the line-of-sight angle to the target aircraft. Eliminating λ_y from Eq. (23) we have

$$H_0 = \lambda_x V/\cos\beta - \lambda_x V_T\cos\gamma_T\tan\beta + 1 + \text{constraints} = 0 \tag{27}$$

Since the constraint terms are always zero, we have from Eq. (27) that

$$\frac{\lambda_x}{\cos\beta} = \frac{-1}{V - V_T\cos\gamma_T\sin\beta} < 0 \tag{28}$$

For intercept to occur, the denominator in Eq. (28) must be positive, which justifies the inequality. Using this condition in Eq. (27) and carrying out the minimization with respect to E and h implied by Eq. (22), we have the following nonlinear solution for the cruise conditions:

$$h_0, E_0 = \arg\{\max_{h,E}\ (V - V_T\cos\gamma_T\sin\beta)\} \tag{29}$$

subject to the constraints in Eqs. (9-11) and (21). It can be shown that Eq. (29) is equivalent to maximizing V subject to the constraints. Thus, the outer solution is independent of intercept geometry and target parameters and need not be computed in flight. This fact is not evident from the solution form given in Eq. (29), since V and β must be regarded as functions of h and E due to the relations in Eqs. (7) and (26).

Having determined the optimal cruise conditions (h_0 and E_0), the optimal cruise velocity V_0 is computed from Eq. (7). Next, the optimal cruise heading (β_0) and the position adjoints are determined from Eqs. (26) and (28). Note that these variables are a function of intercept and target parameters; hence, they must be computed on-line.

First Boundary-Layer Solution

Energy rate dynamics during climb and descent are modeled by introducing the time transformation $\tau_1 = \tau/\epsilon$ and again letting $\epsilon \to 0$ in Eqs. (16) and (18). The necessary conditions for the first boundary layer become:

$$L_{n_1} = 0 \tag{30}$$

$$\partial H_1/\partial h = 0 \qquad \partial H_1/\partial\beta = 0 \qquad \partial H_1/\partial T = 0 \tag{31}$$

$$H_1 = \lambda_{x_0} V\cos\beta + \lambda_{y_0}[V\sin\beta - V_T\cos\gamma_T] + \lambda_E(T - D_0)V/W + 1 + \text{constraints} = 0 \tag{32}$$

where

$$D_0 = qSC_{D_0} + KW^2/qS \tag{33}$$

Note that β dynamics are still taken as instantaneous. From Eqs. (31) and (32) we see that there are four unknowns (h, β, T, λ_E) and four nonlinear equations that must be solved simultaneously. Fortunately, the solution is straightforward. First, we have

$$\partial H_1/\partial\beta = -\lambda_{x_0} V\sin\beta + \lambda_{y_0} V\cos\beta = 0 \tag{34}$$

or

$$\beta_1 = \tan^{-1}\lambda_{y_0}/\lambda_{x_0} = \beta_0 \tag{35}$$

Furthermore, since T appears linearly, we have that

$$T_1 = T_{\max}(hV) \qquad \text{for } \lambda_E < 0 \tag{36}$$

$$T_1 = T_{\min}(h, V) \qquad \text{for } \lambda_E > 0 \tag{37}$$

which correspond to the climb and descent solutions, respectively.

Singular arcs, along which $\lambda_E = 0$ for a finite interval of time, can be excluded by examining the first of Eqs. (18) for $H = H_1$ in Eq. (32).

$$\frac{\mathrm{d}}{\mathrm{d}\tau_1}\lambda_E = \frac{-g(\lambda_{x0}/\cos\beta_0)}{V} > 0 \tag{38}$$

The inequality in Eq. (38) follows from Eq. (28), where we have noted that for intercept to be possible, we must have $(\lambda_{x0}/\cos\beta_0) < 0$.

The minimization with respect to h is obtained by recognizing that $\partial H_1/\partial h = 0$ and $H_1 = 0$ is equivalent to

$$h_1^c = \arg\left\{\min_h\left[\frac{-(T_{\max} - D_0)V/W}{H_0(E,h)}\right]\right\}_{\substack{E=E_{\text{current}} \\ T_{\max}>D}} \tag{39}$$

for climb, and

$$h_1^d = \arg\left\{\min_h\left[\frac{(T_{\min} - D_0)V/W}{H_0(E,h)}\right]\right\}_{\substack{E=E_{\text{current}} \\ T_{\min}<D}} \tag{40}$$

for descent. The term $H_0(E,h)$ in Eqs. (39) and (40) is the outer solution Hamiltonian evaluated at the current values of E, h. These minimizations are subject to the constraints in Eqs. (9-11). Having computed h_1, T_1, and β_1, the adjoint λ_{E_1} is computed using Eq. (32)

$$\lambda_{E_1} = -WH_0(E,h_1)/V_1(T_1 - D_0) \tag{41}$$

Note that since $H_0(E_0,h_0) = 0$ is a minimum for H_0, $H_0(E,h) \geq 0$ and

$$\text{sign}(\lambda_{E_1}) = -\text{sign}(T_1 - D_0) \tag{42}$$

which explains the inequalities in Eqs. (39) and (40).

The solution forms in Eqs. (39) and (40) are dependent on intercept and target parameters due to the presence of H_0 in the denominator. However, it can be shown that equivalent forms for h_1^c and h_1^d are

$$h_1^c = \arg\left\{\min_h\left[\frac{-(T_{\max} - D_0)V}{V - V_0}\right]\right\}_{\substack{E=E_{\text{current}} \\ T_{\max}>D_0}} \tag{43}$$

$$h_1^d = \arg\left\{\min_h\left[\frac{(T_{\min} - D_0)V}{V - V_0}\right]\right\}_{\substack{E=E_{\text{current}} \\ T_{\min}<D_0}} \tag{44}$$

which are independent of geometry and target parameters. This permits preflight calculation of climb and descent paths as functions of energy state. Hence, only λ_{E_1} in Eq. (41) needs to be calculated on-line.

Second Boundary-Layer Solution

Heading rate dynamics are modeled by introducing the time transformation $\tau_2 = t/\epsilon^2$ and letting $\epsilon \to 0$ in Eqs. (16) and (18). The necessary conditions for optimality become

$$\partial H_2/\partial h = 0 \qquad \partial H_2/\partial T = 0 \qquad \partial H_2/\partial L_n = 0 \tag{45}$$

$$H_2 = H_1(E,h,\beta) + \lambda_\beta L_n/mV - \lambda_{E_1} VKL_n^2/qsW + \text{constraints} = 0 \tag{46}$$

where H_1 is given in Eq. (32). Equations (45) and (46) represent four nonlinear equations in four unknowns (h, T, L_n, λ_β).

Assuming that all turning takes place near the initial time at the start of climb, we have $\lambda_{E_1} < 0$. Hence $T_2 = T_{\max}(h_2, V_2)$, where h_2 is the second boundary-layer solution for h and V_2 is computed using Eq. (7) at the current energy level. Using Eq.

(46) and the third variation in Eq. (45), we obtain

$$L_{n_2} = \pm\sqrt{-qsWH_1(E,h,\beta)/VK\lambda_{E_1}} \tag{47}$$

$$\lambda_{\beta_2} = (VKL_{n_2}^2/qsW - H_1)mV/L_n \tag{48}$$

where $\text{sign}(L_{n_2}) = \text{sign}(\beta_0 - \beta)$. The value of h and V needed in Eqs. (47) and (48) is computed using Eq. (41), the first variation in Eq. (45), and the fact that $\text{sign}(\lambda_{\beta_2}) = \text{sign}(L_{n_2})$, which is evident from Eq. (48). These conditions reduce to

$$h_2 = \arg\left\{\min_h \frac{-|L_n|/mV}{H_1(E,h,\beta) - \lambda_{E_1}KL_n^2V/qsW}\right\}_{\substack{E=E_{\text{current}} \\ \beta=\beta_{\text{current}}}} \tag{49}$$

subject to the constraints in Eqs. (9-11).

It is important to note that the forms in Eqs. (43),(44) and (49) avoid having to take partial derivatives with respect to h. Also, Eq. (49) is the only numerical search that needs to be performed on-line. The solution for optimal lift in Eq. (47) is analytic. All second boundary-layer calculations must be performed on-line.

During descent, we set $h_2 = h_1^q(E)$ and use a simple proportional navigation control law to insure intercept in the horizontal plane.

Altitude and Flight-Path Angle Dynamics

Altitude and flight-path dynamics were ignored in the above analysis. As a result, it is necessary to construct feedback control solutions based on the optimality conditions obtained thus far. From the second boundary-layer analysis, we have the component of lift in the horizontal plane (L_{n_2}), the thrust (T_2), which is $T_{\max}$ during ascent and $T_{\min}$ during descent, and the desired altitude (h_2). Hence, we need only construct the component of lift in the vertical plane (L_γ). This will be done such that the aircraft follows h_2 in a reasonable manner.

We first define a desired flight-path angle

$$\gamma_d = \frac{K_1(h_2 - h)}{V} + \dot{E}\frac{\mathrm{d}h_1/\mathrm{d}E}{V_1} \tag{50}$$

The second term in Eq. (50) is based on the $\dot{h}$ equation (3) and the fact that h_1 changes as a function E

$$\gamma_1 \cong \frac{\dot{h}_1}{V} = E\frac{\mathrm{d}h_1/\mathrm{d}E}{V} \tag{51}$$

where $\mathrm{d}h_1/\mathrm{d}E$ is the slope of the optimum climb and descent paths. Then L_γ is computed based on the $\dot{\gamma}$ equation (3) and a desired flight-path angle rate proportional to $(\gamma_D - \gamma)$

$$\dot{\gamma}_d = K_2(\gamma_d - \gamma) = (L_\gamma - W\cos\gamma)/mV \tag{52}$$

Solving for L_γ we have

$$L_\gamma = K_2mV(\gamma_d - \gamma) + W\cos\gamma \tag{53}$$

The controls L and μ are then computed as

$$\mu = \tan^{-1}(L_{n_2}/L_\gamma) \qquad L = L_\gamma^2 + L_{n_2}^2 \tag{54}$$

The constants K_1 and K_2 are chosen to yield a reasonable response time without excessive lift that would result in excessive drag.

Range Matching

It is necessary to determine the point in a trajectory where descent should be initiated in order to arrive at the target altitude when the coordinates in the horizontal plane are driven to zero. This necessitates calculation and storage of descent range and time as a function of energy. For long-range missions that contain a cruise arc, the starting energy for descent is E_0. Descent range and time are given by

$$R_D(E) = \int_{E_0}^{E} \frac{\dot{R}_D}{\dot{E}}(E)\,\mathrm{d}E \qquad t_D(E) = \int_{E_0}^{E} \frac{\mathrm{d}E}{\dot{E}}(E) \tag{55}$$

where

$$\dot{R}_D = V_1(E)\cos\gamma_1(E) \tag{56}$$

$$V_1(E) = \sqrt{(E - h_1^q)2g} \qquad \gamma_1(E) = \sin^{-1}\left[\frac{(\mathrm{d}h_1^q/\mathrm{d}E)\dot{E}(E)}{V_1}\right] \tag{57}$$

In general, the final energy, E_f, is not know a priori and must be determined such that $h(t_f) = h_T(t_f)$. Hence, we must satisfy

$$h_1^q(E_f) = h_T + (V_T\sin\gamma_T)t_D(E_f) \tag{58}$$

at the start of descent. A numerical search is required to find E_f that satisfies Eq. (58). Descent is initiated based on a range-to-go criterion calculated using the current cruise heading and line-of-sight angle. Referring to Fig. 1, we initiate descent when the inequality

$$R_D(E_f)\cos(\beta_0 - \lambda) > R + (V_T\cos\gamma_T\sin\lambda)^*t_D(E_f) \tag{59}$$

is met, where R is current range in the horizontal plane.

In the event that the inequality in Eq. (59) is met before reaching the cruise energy level (e.g., at the start of the trajectory), then it is necessary to constrain E_0 in the outer solution such that the climb range plus the descent range equals the range to intercept.[9] Hence, "pseudo-cruise" energy levels (E_0^*) are defined, each having a separate climb path defined by Eq. (43). The descent paths are all identically the same and need not be recomputed. The value E_0^* is defined by the equality

$$[R_C(E,E_0^*) + R_D(E_f,E_0^*)]\cos(\beta_0 - \lambda) = R + (V_T\cos\gamma_T\sin\lambda)t_{\text{go}} \tag{60}$$

where

$$t_{\text{go}} = t_C(E,E_0^*) + t_D(E_f) - t_D(E_0^*) \tag{61}$$

It is also necessary to modify Eq. (58) in order to predict the intercept energy

$$h_1^q(E_f) = h_T + (V_T\sin\gamma_T)t_{\text{go}} \tag{62}$$

Thus, range matching in the short-range case requires storage of climb distances and times for a family of climb paths corresponding to a range of pseudo-cruise energy levels, the uppermost one corresponding to the unconstrained optimal cruise energy E_0.

Thrust and Lift Control During Descent

Ideally, there should not be a significant amount of maneuvering during descent. However, there is an appreciable amount of turning due to two factors. Since the aircraft velocity varies during descent and the flight-path angle is nonzero, the intercept heading changes from the optimal cruise value. Hence, it is necessary to update the intercept heading during descent. The second factor is due to target maneuvers which occur after descent initiation.

In order to insure intercept, it is necessary to modulate both thrust and the L_n component of lift during descent. In the case of L_n, since $\lambda_{E_1} > 0$ during descent, maximum lift should be employed to maintain intercept heading (note that the quantity under the radical in Eq. (47) becomes negative). However, to avoid oscillations, a proportional control law should be employed when the heading error is small.

Thrust modulations are used to control rate of descent so that the range matching condition is satisfied. Two correction terms are introduced.

$$T = T_{\min} + \delta T_1 + \delta T_2 \tag{63}$$

The first term corrects for the fact that L does not equal W during descent, which is assumed in the R_D and t_D tables. Thus, δT_1 compensates for the increase in drag due to $L > W$

$$\delta T_1 = K(L^2 - W^2)/qs \tag{64}$$

The second component compensates for the current mismatch (δR) in range, where from Eq. (59)

$$\delta R = R + (V_T \cos\gamma_T \sin\lambda) t_{go} - R_D(E, E_f)\cos(\beta_0 - \lambda) \tag{65}$$

where

$$R_D(E,E_f) = R_D(E_f) - R_D(E) \qquad t_{go} = t_D(E_f) - t_D(E) \tag{66}$$

A proportional control law was derived by defining

$$\delta\dot{R} = -K_3 \delta R \tag{67}$$

Noting that

$$\delta\dot{R} = (\mathrm{d}R_D/\mathrm{d}E)\cos(\beta_0 - \lambda)\delta E \qquad \delta\dot{E} = \delta T_2 V/W \tag{68}$$

we can solve for δT_2 as

$$\delta T_2 = \frac{W\delta R}{V\cos(\beta^0 - \lambda)\,\mathrm{d}R_D/\mathrm{d}E} \tag{69}$$

Summary of Control Calculations

A summary of the control calculations is presented in Fig. 2. All on-line calculations are referenced by equation numbers. The purpose of the range matching block is to establish the proper pseudo-cruise point (h_0^*, E_0^*), which may be the optimal cruise for long-range missions. During climb, the costates are calculated on-line and h_1^c is available from the climb table corresponding to the cruise energy E_0^*. All turn parameters must be calculated on-line. During descent, h_1^d is taken from the descent table (which is independent of E_0^*), and thrust and lift are computed as described above.

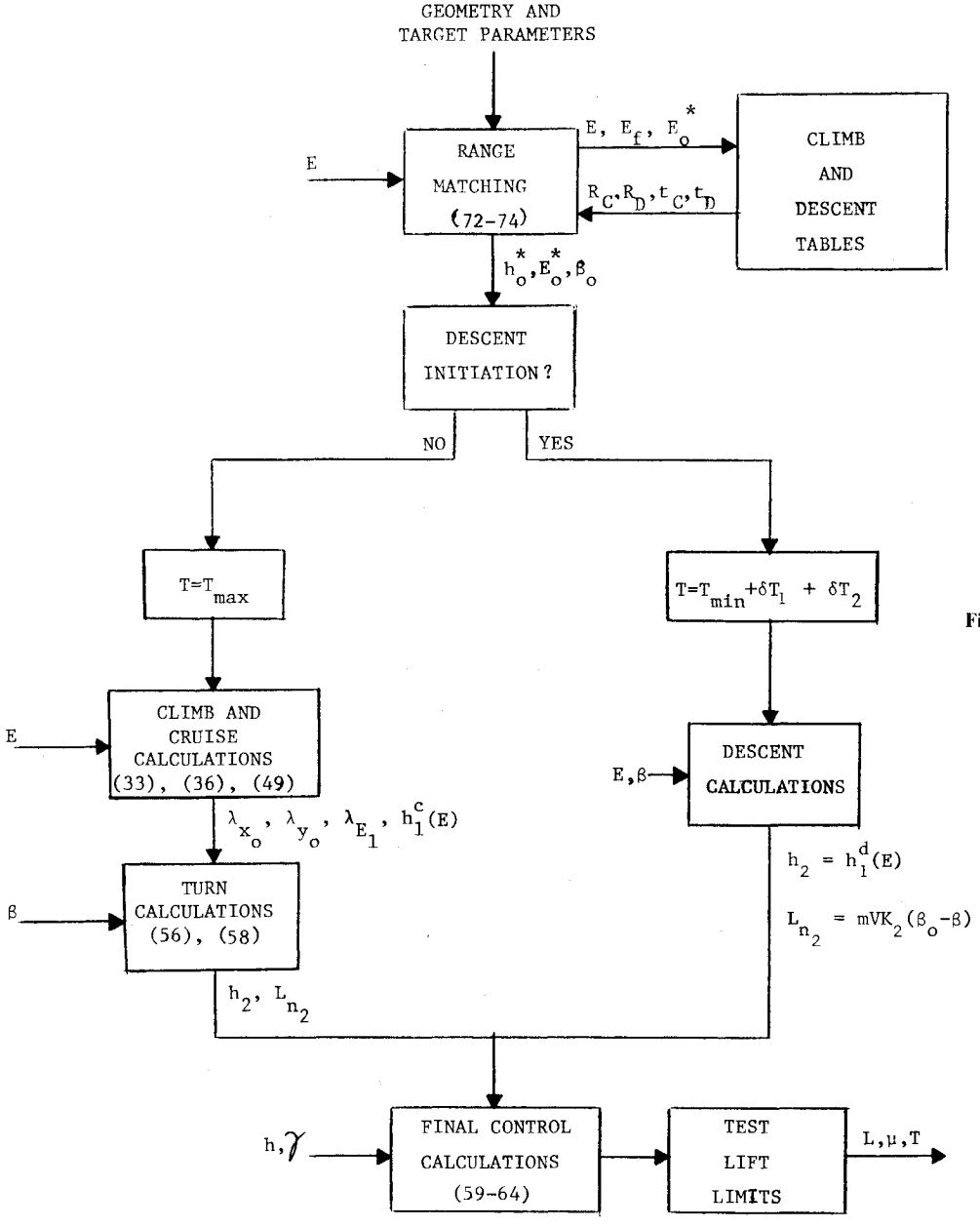

Fig. 2 Summary of control calculations.

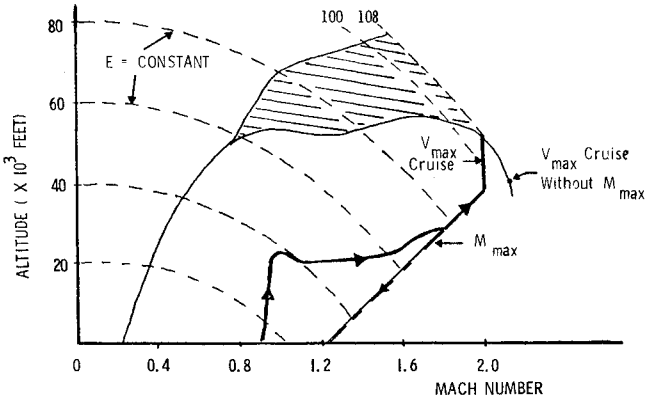

Fig. 3 Aircraft flight envelope.

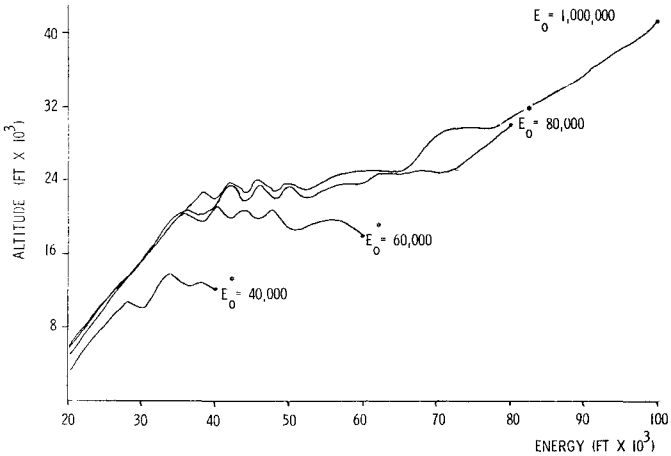

Fig. 4 Climb paths to several cruise energies.

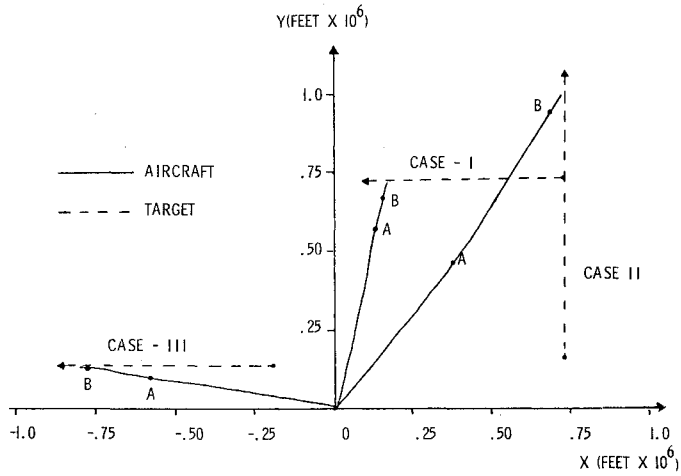

Fig. 5 Horizontal plane projection of aircraft and target motion.

Numerical Results

The aircraft simulated in this study is an early version of the F-4 used by Bryson et al.[1] as airplane 1. The computer used in this numerical study is an IBM 370/168. This machine has a 32-bit word size, a basic machine cycle time of 8 ns and performs 3×10^6 floating point operations per second. Main storage access time averages 480 ns. With this machine, the control computations occupied approximately 3% of the trajectory time using a control update rate of 0.5 s, and 43,721 bytes in core.

The aircraft flight envelope is shown in Fig. 3. The uppermost line corresponds to the conditions $qsC_{L_{max}} = W$. The shaded area is a region of negative energy rate. The Mach limit is a scheduled function of altitude up to $h = 38{,}000$ ft. Above this altitude, $M_{max} = 2$. The dynamic pressure limit does not play a role in this case and $G_{max} = 4.0$, $\alpha_{max} = 12$ deg.

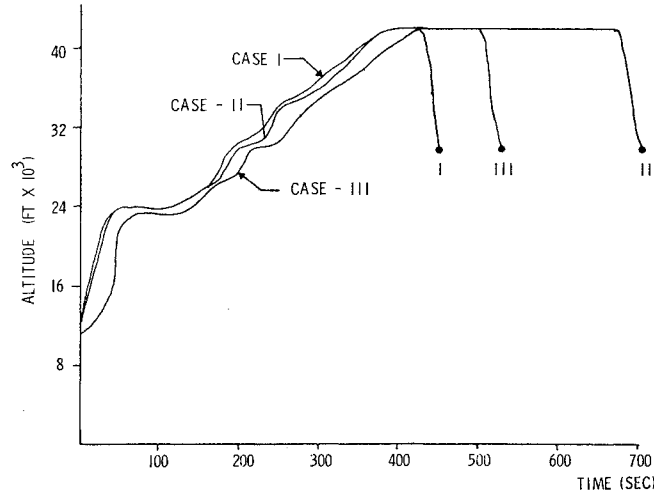

Fig. 6 Altitude profiles for cases I, II, and III.

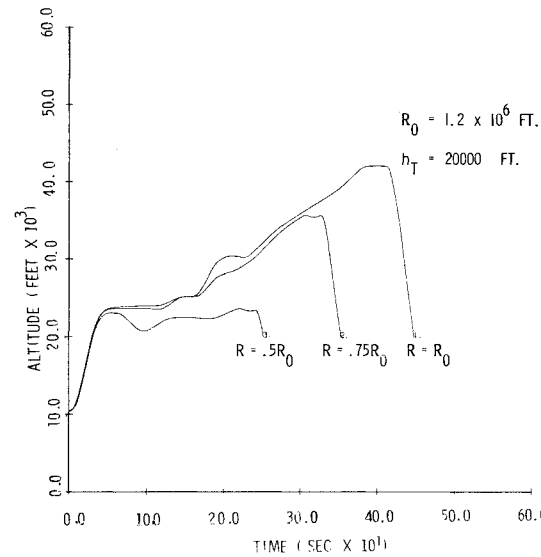

Fig. 7 Altitude profiles for case I for several values of initial range.

The bold line corresponds to $h_f^c(E)$ for the long-range case. It is evident that, due to the M_{max} constraint its invariancy at high altitudes, the optimal cruise point is nonunique. Note that V_{max} remains constant within 12,000 ft of the aircraft's operating ceiling. The optimum descent path lies directly along the Mach limit in this case. In this study, the long-range cruise point was taken at 42,000 ft to avoid an unnecessary climb and descent in the region above this altitude.

The optimal climb paths to several pseudo-cruise energy levels are shown in Fig. 4. It is evident that in all cases there is an interval of "ripples" in the altitude schedule for climb, although little change occurs in the average altitude in this region. This region is due to the fact that the function in Eq. (43) has a flat minimum with respect to h over the range $35{,}000 < E < 50{,}000$ ft. Thus, optimality is insensitive to the value of h_f^c selected in this region. This phenomenon had negligible effect on the trajectories and flight times, but did have an observable effect on lift and bank angle histories.

Figure 5 shows the horizontal plane projection of three profiles generated using the point mass equations of motion in Eqs. (1-3). In all cases, the target altitude and velocity are constant at 3×10^4 ft and 1200 ft/s, respectively. The starting altitude and velocity for the controlled aircraft are 10,420 ft and 863 ft/s, and the initial heading is along the x axis.† The target trajectory is shown dashed. Note that it is impossible to discern the initial turn to the intercept path on this scale, which graphically illustrates the speed of turning dynamics in

†Note that the coordinate frame here is inertially fixed and does not correspond in that of Fig. 1.

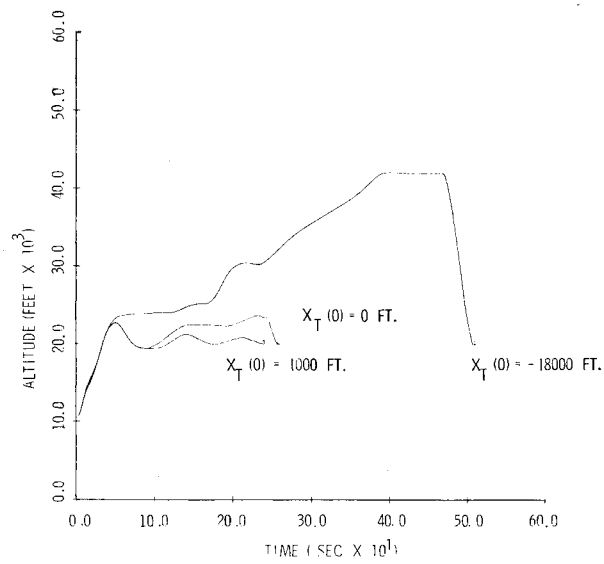

Fig. 8 Altitude profiles for case III for several values of $x_T(0)$.

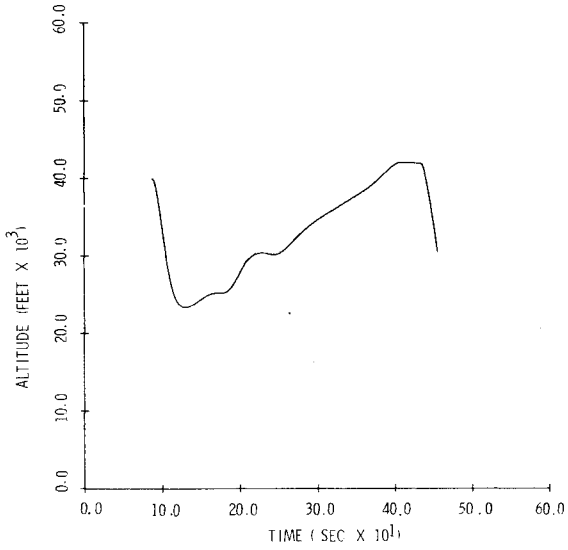

Fig. 9 Transition to climb for case I.

relation to energy and relative position dynamics. The points labeled A and B correspond to the start and end of cruise.

The corresponding altitude profiles are shown in Fig. 6. Note that in cases I-III, the optimal cruise altitude of 42,000 ft was reached. Hence, in these cases, $h_1^c(E)$ corresponding to $E_0 = 100{,}000$ ft was used. The varying altitude profiles are due to the different amount of turning required in each case.

Figure 7 shows the effect that changing the initial range (R_0) has on the altitude profile for case I. For shorter initial ranges, the optimal profiles do not attain the long-range cruise energy level. Figure 8 shows the same effect for case III brought about by changing the x coordinate of initial target position. Figure 9 illustrates an initial transition to the optimal climb path. This case was generated by taking the conditions of case I at 87.0 s and moving the aircraft altitude to 40,000 ft, holding total energy constant. This transition illustrates the effectiveness of the suboptimal control law in Eq. (53) in attaining the desired altitude and flight-path angle.

Concluding Remarks

It has been demonstrated that singular perturbation methods are an effective tool for developing computer algorithms for on-line optimal aircraft controls. The computation time and storage requirements are well within the capabilities of present-day flight computers. This evaluation is based on a minimum time intercept problem. Extensions to other performance indices and other forms of terminal constraints should be possible. Extensions of the analysis on the current problem should include optimization of altitude and flight-path dynamics, modeling aircraft weight variations, and correction of the solutions to first order in energy. In particular, the optimal cruise heading should be corrected for velocity and flight-path angle variations that take place during descent.

The assumptions regarding the separation and ordering of times scales made in this paper impose restrictions on the range of applicability of the resulting solutions. Although this is difficult to quantify, the following comments are offered:

1) The range to intercept must be sufficiently large so that the optimal profiles are characterized by climbs and descents, with the addition of a cruise leg in the long-range case. If the heading error is zero, any range greater than the range used in descending to the target altitude from the current energy is permissible. Shorter ranges will result in the need for a zoom dive.

2) The target altitude at intercept is assumed to be less than the altitude in the descent table corresponding to the cruise energy selected by the range matching logic. Higher-altitude targets can be accommodated by ending the climb with a zoom transition.

3) At short ranges and large heading errors, the energy rate and heading rate dynamics become highly coupled, especially in the case of a maneuvering target. When the optimal pursuit path is dominated by turning, then the ordering of energy rate and turn rate dynamics should be reversed.

Appendix: Ordering of Energy and Heading Dynamics

This appendix provides further justification for the ordering selected for energy and heading dynamics. In particular, the ordering here is the reverse of that taken in several earlier papers[2,4,5] and some resolution is in order.

Of interest are the eigenvalues associated with a linearized boundary-value problem in which E and β dynamics are taken on the same time scale. In this case, the necessary conditions during climb are

$$H = \lambda_{x_0} V\cos\beta + \lambda_{y_0}(V\sin\beta - V_T\cos\gamma_T) + \lambda_E(T_{\max} - D)V/W + \lambda_\beta L_n/mV + 1 + \text{constraints} = 0 \quad \text{(A1)}$$

where λ_{x0}, λ_{y0}, V_0, and β_0 are determined by Eqs. (26-29). The remaining necessary conditions are‡

$$E' = (T_{\max} - D)V/W \qquad \lambda_E' = -\partial H_1/\partial E \quad \text{(A2)}$$

$$\beta' = L_n/mV \qquad \lambda_\beta' = -\partial H_1/\partial\beta \quad \text{(A3)}$$

$$\partial H/\partial h = 0 \qquad \partial H/\partial L_n = 0 \quad \text{(A4)}$$

where for

$$D = D_0 + KL_n^2/qs \quad \text{(A5)}$$

the second of Eqs. (A4) gives

$$L_n = (\rho sg/4K\lambda_E)\lambda_\beta \quad \text{(A6)}$$

Consider an expansion of the above conditions about the optimal climb solution for $\tilde{\beta} = \beta_0$, where we also have

$$\tilde{\lambda}_E = \lambda_{E_1}(E) \qquad \tilde{\lambda}_\beta = 0 \qquad \tilde{h} = h_1(E)$$
$$\tilde{E}' = \dot{E}_1(E) \qquad \tilde{L}_n = 0 \qquad \partial H_1/\partial h = 0 \quad \text{(A7)}$$

‡The prime in Eqs. (A2) and (A3) denotes $d/d\tau_1$.

Table 1 Comparison of eigenvalues during climb for case 1

Energy level, ft	P_E, 1/s	P_β, 1/s
22,000	±0.0200	±0.317
40,000	±0.0186	±0.178
60,000	±0.00230	±0.164
80,000	±0.00900	±0.152
98,000	±0.00115	±0.763
100,000	0[a]	∞[a]

[a] For the F-4, $\partial \dot{E}_1/\partial E = \lambda_{E_1} = 0$ in cruise due to the Mach limit.

In Eq. (47), all the nominal values are those associated with the first boundary-layer analysis of this paper. The linearized dynamics resulting from Eqs. (A2-A6) are

$$\delta E' = (\partial E'/\partial E)\delta E + (\partial E'/\partial h)\delta h = (\partial \dot{E}_1/\partial E)\delta E \qquad \text{(A8a)}$$

$$\delta \lambda_E' = -(\partial \dot{E}_1/\partial E)\delta \lambda_E + f(E,\bar{h})\delta E \qquad \text{(A8b)}$$

$$\delta \beta' = (\bar{\rho} sg/\lambda_{E_1} Km V_1)\delta \lambda_\beta \qquad \text{(A9a)}$$

$$\delta \lambda_\beta' = (\lambda_{x_0}/\cos\beta_0) V_1 \delta\beta \qquad \text{(A9b)}$$

where we have eliminated δh using the first of Eqs. (A4). The function $f(E,\bar{h})$ is, in general, complicated to evaluate, but does not affect the eigenvalues of Eqs. (A8). Note that Eqs. (A8) and (A9) are decoupled. The eigenvalues of Eqs. (A8) are

$$P_E = \pm(\partial \dot{E}_1/\partial E) \qquad \text{(A10)}$$

and for Eqs. (A9) we have

$$P_\beta = \pm\sqrt{(\lambda_{x_0}/\cos\beta_0)\bar{\rho} sg/\lambda_{E_1} Km} \qquad \text{(A11)}$$

where $\lambda_{x_0}/\cos\beta_0$ and λ_{E_1} are computed using Eqs. (28) and (41), and both are negative. In the case where relative position dynamics are ignored,[2,4,5] we have that $\lambda_{x_0} = 0$ and E is selected as the faster variable. However, in this case, β is clearly the faster variable, as is evidenced by the numerical values of P_E and P_β for the F-4 given in Table 1, for case I of the section on Numerical Results.

Acknowledgments

The author wishes to acknowledge the support provided by Daniel Moerder in generating the numerical results presented in this paper. This research was supported by NASA Langley Research Center under Grant No. NSG-1496.

References

[1] Bryson, A.E., Desai, M.N., and Hoffman, W.L., "The Energy State Approximation in Performance Optimization of Supersonic Aircraft," *Journal of Aircraft,* Vol. 6, Nov.-Dec. 1969, pp. 481-487.

[2] Hendrick, J.K. and Bryson, A.E., "Three-Dimensional, Minimum-Time Turns for a Supersonic Aircraft," *Journal of Aircraft,* Vol. 9, Feb. 1972, pp. 115-121.

[3] Parsons, M.G., Bryson, A.E., and Hoffman, W.E., "Long-Range Energy-State Maneuvers for Minimum Time to Specified Terminal Conditions," AIAA Paper No. 73-229, 11th Aerospace Sciences Meeting, Jan. 1973; also *JOTA,* Vol. 17, 1975, pp. 447-463.

[4] Kelley, H.J. and Lefton, L., "Supersonic Aircraft Energy Turns," presented at the Fifth IFAC Conference, Paris, France, June 1972; also *Automatica,* Vol. 8, p. 575.

[5] Calise, A.J., "Extended Energy Management for Variational Problems in Aircraft Flight," *AIAA Journal,* Vol. 15, March 1977, pp. 314-321.

[6] Calise, A.J., "Singular Perturbation Methods for Variational Problems in Aircraft Flight," *IEEE Transactions on Automatic Control,* Vol. AC-21, June 1976, pp. 345-353.

[7] Calise, A.J., "Singular Perturbation Analysis of Optimal Thrust Control with Proportional Navigation Guidance," *Journal of Guidance and Control,* Vol. 4, July-Aug. 1980, pp. 312-318.

[8] Washburn, R.B., Mehra, R.K., and Sajan, S., "Application of Singular Perturbation Techniques and Continuation Methods for On-line Aircraft Trajectory Optimization," *Proceedings of the Conference on Decision and Control,* San Diego, Calif., Jan. 1979, pp. 983-990.

[9] Calise, A.J., "A New Boundary Layer Matching for Singularly Perturbed Systems," *IEEE Transactions on Automatic Control,* Vol. AC-23, June 1978, pp. 434-438.